Contrib Mineral Petrol (1996) 124:359–369

Gregory M. Yaxley · David H. Green

Experimental reconstruction of sodic dolomitic carbonatite melts from metasomatised lithosphere

Received: 15 December 1995/Accepted: 14 February 1996

Abstract Investigations of peridotite xenolith suites have identified a compositional trend from lherzolite to magnesian wehrlite in which clinopyroxene increases at the expense of orthopyroxene and aluminous spinel, and in which apatite may be a minor phase. Previous studies have shown that this trend in mineralogy and chemical composition may result from reaction between sodic dolomitic carbonatite melt and lherzolite at pressures around 1.7 to 2 GPa. This reaction results in decarbonation of the carbonatite melt, releasing CO_2-rich fluid. In this study, we have experimentally reversed the decarbonation reaction by taking two natural wehrlite compositions and reacting them with CO_2 at a pressure of 2.2 GPa and temperatures from 900 to 1150° C. Starting materials were pargasite-bearing wehrlites, one with minor apatite (composition 71001*) and one without apatite (composition 70965*). At lower temperatures (900° C) the products were apatite + pargasite + magnesite harzburgite for runs using composition 71001*, and pargasite + dolomite lherzolite for runs using composition 70965*. At and above 1000° C, carbonatite melt with harzburgite residue (olivine + orthopyroxene + spinel) and with lherzolite residue (olivine + orthopyroxene + clinopyroxene + spinel) were produced respectively. Phase compositions in reactants and products are consistent with the documented carbonatite/lherzolite reactions, and also permit estimation of the carbonatite melt compositions. In both cases the melts are sodic dolomitic carbonatites. The study supports the hypothesis of a significant role for ephemeral, sodic dolomitic melts in causing metasomatic changes in the lithosphere at $P \leq 2$ GPa. The compositions of wehrlites imply fluxes of CO_2, released by metasomatic reactions, which are locally very large at around 5 wt% CO_2.

G.M. Yaxley (✉) · D.H. Green
Research School of Earth Sciences, The Australian National University, Canberra ACT 0200, Australia

Editorial responsibility: J. Hoefs

Introduction

High pressure experimental studies of hydrous, carbonate-bearing fertile peridotite compositions have led to the discovery that high Mg# [where Mg# $= 100\ \mathrm{Mg}/(\mathrm{Mg} + \sum\mathrm{Fe})$] dolomitic carbonatite melts may form as low degree primary melts in equilibrium with pargasite-bearing spinel or garnet lherzolite from 2.1 to 3.1 GPa and 980 to 1080° C (Wallace and Green 1988; Falloon and Green 1990; Thibault et al. 1992).

Carbonatite melts are believed to be capable of forming an interconnected grain boundary network in an olivine-dominated matrix at very low melt fractions of $\ll 1\%$ (Hunter and MacKenzie, 1989). Coupled with their low density and viscosity, this may permit rapid and pervasive ascent from their source regions (Hunter and MacKenzie 1989; Watson et al. 1990). This behaviour, together with their large ion lithophile element (LILE)-enriched nature, may make carbonatite melts effective as metasomatic agents in the lithosphere (Green and Wallace 1988). Such melts, on ascending from their source regions through cooler lithosphere, could eventually cross the carbonated peridotite solidus at pressures less than the decarbonation reaction orthopyroxene (opx) + dolomite = olivine + clinopyroxene (cpx) + CO_2, resulting in conversion of refractory spinel lherzolite or harzburgite to magnesian wehrlite mineralogy with or without low-Ti pargasite, accompanied by release of a CO_2-rich fluid (Green and Wallace 1988; Yaxley et al. 1991). Evolution of the reacting carbonatite may result in increasing P_2O_5 + halogen and H_2O contents, possibly forming a late-stage saline melt or "brine" from which accessory apatite is deposited. The carbonatite is "ephemeral" in the sense that it is absorbed by the lithosphere, with release of ≈ 50 wt % of $CO_2 \gg H_2O$ fluid. The melt components other than CO_2 are fixed in the lithosphere as increased clinopyroxene and as pargasitic amphibole and apatite. The result of these mineralogical changes would be to drive the bulk-rock

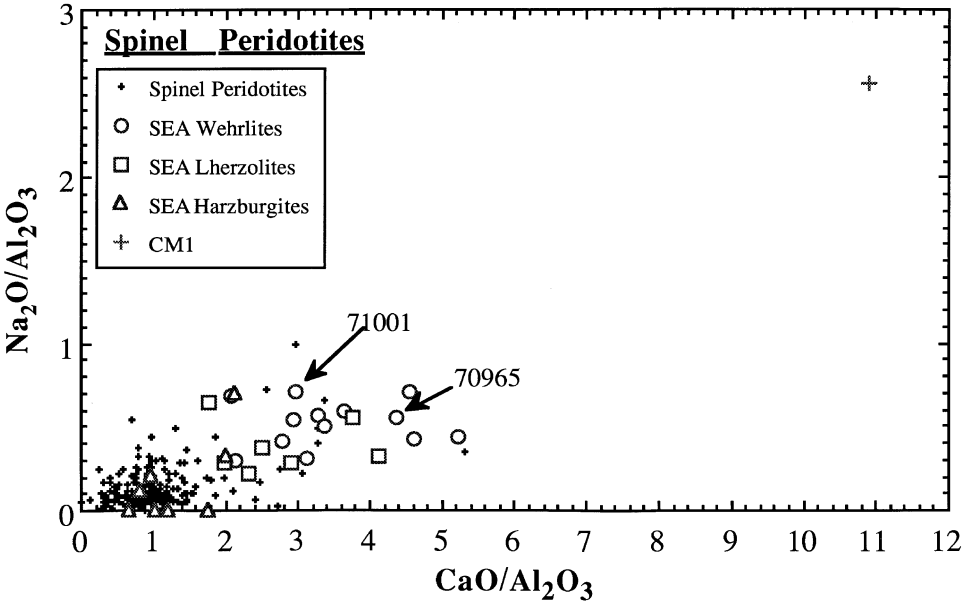

Fig. 1 Plot of CaO/Al_2O_3 versus Na_2O/Al_2O_3 for around 300 spinel peridotite xenoliths from localities around the world (*black crosses*) (data sources available from the authors), and the southeastern Australian (SEA) carbonatite-metasomatised suite of Yaxley et al. (1991) and G.M. Yaxley (unpublished data). The compositions of the starting mixes (71001 and 70965) used in the experiments described herein are indicated, as is the experimental primary carbonatite melt composition (CM1) estimated by Wallace and Green (1988). See text for further explanation

geochemistry of affected parts of the lithosphere towards high Ca/Al and Na/Al values (Fig. 1), high P_2O_5 abundances, and moderate to extreme LILE enrichment decoupled from Ti abundances (Green and Wallace 1988).

These mineralogical and geochemical characteristics have been documented in recent studies of spinel peridotite xenoliths from southeastern Australia (Yaxley et al. 1991), Saharan Africa (Dautria et al. 1992), the Eifel region of Germany (Thibault et al. 1992) and the Kaapvaal craton, southern Africa (Rudnick et al. 1992, 1993). Yaxley et al. (1991) concluded that the apatite-bearing southeastern Australian magnesian wehrlites represented the end-product of carbonatite metasomatism, in which all primary orthopyroxene had reacted out, followed by annealing to an olivine + clinopyroxene dominated assemblage.

In order to test the above model, a series of high pressure experiments was performed which aimed to demonstrate that the compositions of two of the southeastern Australian magnesian wehrlite (orthopyroxene-absent) nodules described by Yaxley et al. (1991) are consistent with the metasomatic addition of an ephemeral sodic dolomitic melt to an orthopyroxene-bearing spinel peridotite assemblage, resulting in decarbonation and replacement of orthopyroxene by clinopyroxene. This was achieved by effectively reversing the natural metasomatic process, by running hydrous (≈ 0.5 wt % H_2O), synthetic compositions equivalent to those of 71001 and 70965 (minus 40% olivine) (Yaxley et al. 1991) in the presence of 1, 5 or 7 wt% CO_2, at a range of *PT* conditions which span the carbonatite melt field in the fluid undersaturated pyrolite-CO_2-H_2O system (Wallace and Green 1988). This produced carbonatite melt in equilibrium with harzburgite or lherzolite residue, and allowed estimates of the composition of the postulated natural, metasomatizing carbonatite to be made. Implicit to the approach is an assumption that apart from released CO_2- (and possibly H_2O-) bearing fluid or fluids, the pre-existing lherzolite has undergone simple bulk mixing with the invasive carbonatite melt, i.e. the metal oxide components of the carbonatite have been absorbed more or less completely by the wall-rock. More realistically, carbonatite metasomatism probably involves "open-system" behaviour, understanding of which requires knowledge of partitioning relationships between carbonatite melts and mantle lherzolite minerals (olivine, orthopyroxene, clinopyroxene, spinel, garnet, amphibole, phlogopite, apatite) and the possible identification of low temperature H_2O-rich, "brine" coexisting with CO_2-rich fluid. Our experiments explore a scenario in which only CO_2 is assumed to be lost from the carbonatite + lherzolite reaction.

Experimental details

Choice and preparation of starting materials

The compositions of samples 71001 and 70965 (Yaxley et al. 1991) were chosen for the experimental investigation. Both fulfill the carbonatite metasomatic characteristics described previously, but they also exhibit significant differences in their geochemistry. For example, 70965 has a significantly higher CaO/Al_2O_3 ratio (4.38 cf. 2.96) at similar Al_2O_3 contents, but slightly lower Na_2O/Al_2O_3 (0.55 cf. 0.71). The P_2O_5 content is much higher in 71001 (0.77 cf. 0.02 wt %) and this is reflected in the modal apatite contents of the natural assemblages; 70965 is free of detectable modal apatite, whereas it is abundant in 71001. Least squares mass balance calculations performed on the bulk and mineral compositions of *nodule* 71001 indicate an apatite content of 2.2 modal% in the natural rock.

Synthetic amphibole-bearing wehrlites with the same compositions as samples 71001 and 70965 (− 40% olivine of ambient mol%

forsterite)[1] were prepared from high purity oxides and carbonates which were ground under AR quality acetone for several hours to ensure homogeneity. These starting mixes were fired in ≈ 100 mg aliquants for 48 hours with excess water at 1.5 GPa and 925° C (sub-solidus), producing an olivine + clinopyroxene + pargasite + Cr-spinel + apatite assemblage (71001*), and an olivine + clinopyroxene + pargasite + Cr-spinel assemblage (70965*). No orthopyroxene was detected in either composition after extensive examination of synthesis run products under refractive index oils, or with the electron microprobe. Determination of phase compositions and least squares mass balance calculations enabled calculation of modal proportions (Table 1). Examination of powdered run material suspended in immersion oils under transmitted light, and of polished sections under the SEM and electron microprobe qualitatively confirmed the modal analyses. Excess water was observed bubbling from the pierced capsules after all synthesis runs, indicating that water saturation was achieved. Run material was ground to < 10 μm under acetone, and then dried for several hours at 400° C in argon. In composition 71001*, the calculated modal amphibole content is 19.8%, with an apatite content of 3.12%. Assuming stoichiometric water in these two hydrous phases, then the bulk water content of 71001* is approximately 0.5 wt%. The 70965* composition contains 0.4 wt % H_2O and substantially higher modal clinopyroxene (22.7 cf. 5.4% in 71001*) reflecting its significantly greater CaO content and Ca/Al value. The bulk and modal compositions are presented in Table 1.

Table 1 Bulk compositions (nominal) for starting mixes used in these experiments. Modal proportions were determined by least squares mixing of bulk and individual phase compositions

	71001 − 40% Olivine	70965 − 40% Olivine
SiO_2	41.50	45.89
TiO_2	0.17	0.13
Al_2O_3	1.55	1.65
∑FeO	9.70	7.35
MnO	0.30	0.25
MgO	38.93	35.51
CaO	4.59	7.21
Na_2O	1.10	0.91
K_2O	0.12	0.05
Cr_2O_3	0.76	0.86
NiO	–	0.02
P_2O_5	1.30	0.03
Total	100.00	99.85
Mg#	87.74	89.60
Olivine	70.87	55.77
Clinopyroxene	5.35	22.72
Spinel	0.84	0.11
Amphibole	19.82	21.40
Apatite	3.12	0.00
$\sum r^2$	0.12	0.68

Experimental runs

Aliquants of the synthetic wehrlites, together with sufficient silver oxalate ($Ag_2C_2O_4$) to decompose to 1, 5 or 7 wt % CO_2 (total mass around 15 mg) were loaded into welded 2.2 mm outside diameter (OD) $Ag_{75}Pd_{25}$ or $Ag_{70}Pd_{30}$ capsules. A small disc of pre-fractured San Carlos olivine (Mg# = 89) was placed near the top of the capsule, to trap any melt as inclusions. In some runs, a layer of coarsely crushed San Carlos olivine was used in the same manner. The base of the capsule was maintained at $T < 100$° C during welding to minimize premature decomposition of the $Ag_2C_2O_4$. The small capsule was surrounded by natural magnesite in a welded 3.5 mm OD $Ag_{50}Pd_{50}$ or Pt outer capsule. The buffering reaction,

$$(1)\ MgCO_3 = MgO + C + O_2$$

ensured carbonate stability during runs by maintaining oxygen fugacity (fO_2) ≈ EMOG (Eggler and Baker 1982).

Experiments were run in a 1.27 cm diameter high pressure piston-cylinder apparatus at the University of Tasmania. Sodium chloride or NaCl-pyrex assemblies were used with graphite heaters. Pressures are accurate to ±0.1 GPa. Temperature was controlled to an accuracy of ±10° C, and precision of ±1° C with a $Pt/Pt_{90}Rh_{10}$ thermocouple attached to a Eurotherm 818P solid-state controller. Run times varied from 2 to 168 hours.

Analytical details

Run products and residual buffer material were examined optically under immersion oils of accurately known refractive index in order to identify phases and to ensure that buffer exhaustion had not occurred. Run material was mounted in epoxy and polished in water-free oils to prevent dissolution of any carbonate phases (Wallace and Green 1988). These mounts were used for Scanning Electron Microscopy (SEM) on a Phillips 505 SEM, and electron probe microanalysis. In addition, unpolished fragments of run material from several runs were examined under the SEM to check for loss of carbonate quench phases during polishing.

Electron probe microanalyses were performed at the University of Tasmania on a Cameca SX50 electron microprobe which was calibrated using natural mineral standards. Data was processed using PAP matrix correction methods. Count times were 10 to 30 seconds on peaks, and 5 to 15 seconds on background, depending on the element's concentration. An accelerating voltage of 15 kV, and beam currents of 10 (carbonate analyses) or 20 nA (silicates + spinel + apatite analyses) were used.

Phase equilibration in runs appears to have been closely approached, based on homogeneity of multiple analyses of silicate phases. The Fe-loss was minimized by the use of $Ag_{75}Pd_{25}$ or $Ag_{70}Pd_{30}$ capsules. Retention of initial Fe-content was confirmed by lack of zoning in olivine grains, and by Mg#s of phases and bulk compositions.

Experimental results

Phase assemblages

Details of run conditions, and phases detected in each run are presented in Table 2, with representative microprobe analyses in Tables 3 to 5. The experimental runs produced carbonate-bearing harzburgitic (71001*) or lherzolitic (70965*) assemblages. The presence of pargasite and the nature of the carbonate distinguished sub-solidus from above-solidus experiments. Despite its presence in the amphibole-wehrlite starting material, clinopyroxene was absent in all CO_2-bearing runs using composition 71001*, and decreased in abundance in 70965* runs. Orthopyroxene was present in all CO_2-bearing runs with both bulk compositions,

[1] The olivine-depleted compositions synthesised are designated 71001* and 70965*.

Table 2 Summary of runs and products. Wt% CO_2 quoted on a "weighed in" basis, and represents maximum values due to possible minor decomposition of $Ag_2C_2O_4$ on welding. [*OL* olivine, *OPX* orthopyroxene, *CPX* clinopyroxene, *AP* apatite, *AM* amphibole, *SP* spinel, *MAG* sub-solidus magnesitic carbonate, *DOL* subsolidus dolomitic carbonate, *CBTE* quenched carbonate melt, *GL* quenched silicate melt (glass)]

Run no.	Pressure (GPa)	Temperature (°C)	Run time (h)	CO_2 (wt%)	Phases	Comment
Composition 71001*						
T-3149	1.5	925	48	0.00	OL + CPX + AM + AP + SP	H_2O excess synthesis run
T-3301	2.2	900	117	0.97	OL + OPX + AM + AP + SP + MAG	Sub-solidus
T-3172	2.2	900	48	4.31	OL + OPX + AM + AP + SP + MAG	Sub-solidus
T-3170	2.2	1000	24	5.28	OL + OPX + SP + CBTE	In carbonatite melt field
T-3690	2.2	1000	168	5.00	OL + OPX + SP + CBTE	Unpolished
T-3197	2.2	1050	24	5.09	OL + OPX + SP + CBTE	In carbonatite melt field
T-3491	2.2	1070	25	4.43	OL + OPX + SP + CBTE	In carbonatite melt field
T-3188	2.2	1100	2	7.24	OL + OPX + GL	Silicate melt field
Composition 70965*						
T-3309	1.5	925	48	0.00	OL + CPX + AM + SP	H_2O excess synthesis run
T-3482	2.2	900	120	1.06	OL + OPX + CPX + AM + SP + DOL	Sub-solidus
T-3315	2.2	900	116	4.60	OL + OPX + CPX + AM + SP + DOL	Sub-solidus
T-3627	2.2	1000	168	5.00	OL + OPX + CPX + SP + CBTE	Unpolished
T-3447	2.2	1000	25	4.49	OL + OPX + CPX + SP + CBTE	In carbonatite melt field
T-3560	2.2	1050	160	5.00	OL + OPX + CPX + SP + CBTE	In carbonatite melt field
T-3327	2.2	1050	24	4.50	OL + OPX + CPX + SP + CBTE	In carbonatite melt field
T-3586	2.2	1050	60	7.00	OL + OPX + CPX + SP + CBTE	In carbonatite melt field
T-3469	2.2	1070	24	4.43	OL + OPX + CPX + SP + CBTE	In carbonatite melt field
T-3336	2.2	1150	2	4.92	OL + OPX + CPX + GL	Silicate melt field

despite being absent in the synthetic amphibole-wehrlite starting materials.

Although the exact position of the solidus was not determined for these compositions, the sub- or super-solidus position of each run was delineated using the textures of carbonate phases found in the runs. For example, super-solidus runs contained carbonate with distinctive quench textures comprised of acicular to tabular dolomite, and delicate needles of (Na, Mg)-carbonate (Fig. 2). Carbonate in sub-solidus runs did not display quench-like textures. On this basis, the solidus was determined to lie between 900 and 1000° C at 2.2 GPa for both bulk compositions.

Euhedral laths of pargasitic amphibole were present in runs at 900°C (sub-solidus) for both compositions, but were not detected in runs at $T > 900°$ C (super-solidus) in either composition. Apatite was present in sub-solidus runs but absent in super-solidus runs for composition 71001*. No run using 70965* contained detectable apatite.

Silicate, spinel and apatite mineralogy

Olivine compositions (Table 3) ranged from 87.9 to 88.4 mol% forsterite (71001*) and 89.3 to 90.3 mol % forsterite (70965*). No systematic increase in Fo content was observed when crossing the solidus into the carbonate melt field, consistent with the observations of Wallace and Green (1988), and Thibault et al. (1992). Similarly, the Mg# of orthopyroxene in 71001*, and orthopyroxene and clinopyroxene in 70965* did not increase systematically with temperature (Table 3). In most cases, pyroxene Mg#s were slightly higher than Fo contents in co-existing olivines.

The presence of orthopyroxene + carbonate melt in runs at 1000° C or more, suggests that reversal of the postulated metasomatic reaction orthopyroxene + dolomitic melt = olivine + clinopyroxene + CO_2-rich fluid, has occurred. In 71001*, clinopyroxene was eliminated in super-solidus runs, suggesting that CO_2 was in excess. (all experiments contained $> 4\%$ CO_2). The retention of clinopyroxene in 70965* super-solidus runs suggests that the pre-metasomatic natural rock was lherzolite, or that 5 or even 7 wt% CO_2 was not sufficient to completely reverse the process if the precursor rock was harzburgite. This is supported by the presence of spheroidal vapour holes in 71001* run material (Fig. 2a), which were absent in 70965* runs. It is also consistent with the much higher Ca/Al value of 70965* compared with 71001*, despite the former's lack of modal apatite.

Calcic amphibole was found in all sub-solidus runs for both starting mix compositions as tabular grains up to 10 μm in length. It has a rather unusual, broadly edenitic hornblende to edenitic composition, rather than pargasitic, due mainly to low Al content (Table 4). For example, in 71001* runs, amphibole was Al-deficient, containing no octahedral Al (Al^6), and only about 1.1–1.2 Al^4 cations per 8 oxygen anions. In runs using 70965*, amphibole contained about 0.03–0.09 Al^6 cations per 8 oxygen anions, and similar levels of Al^4 to those in 71001* runs.

Fig. 2A–C Back scattered electron images of **A** unpolished material from run T-3690 (71001), showing abundant spheroidal cavities indicative of the presence of a free fluid phase. In addition, needles of quenched (Na,Mg)-carbonate are visible. **B** Closer view of quenched carbonatite in T-3690. Needles are (Na,Mg)-carbonate. Small euhedral white grains are dolomite. **C** Carbonatite melt trapped in annealed layer of coarse San Carlos olivine grains which were included in T-3586. Quench structures are clearly visible

Yaxley et al. (1991) proposed a series of carbonatite metasomatic end-member reactions between sodic dolomitic melt and lithospheric wall-rock phases

(2) $4MgSiO_3 + CaMg(CO_3)_2 = 2Mg_2SiO_4 + CaMgSi_2O_6 + 2CO_2$

enstatite dolomite forsterite diopside

(3) $[7MgSiO_3 + MgAl_2SiO_6] + Na_2CO_3$

enstatite Mg-Tschermaks sodium carbonate

$= 4Mg_2SiO_4 + 2NaAlSi_2O_6 + CO_2$

forsterite jadeite

(4) $9MgSiO_3 + Mg(Cr,Al)_2O_4 + Na_2CO_3$

enstatite spinel sodium carbonate

$= 5Mg_2SiO_4 + 2Na(Cr,Al)Si_2O_6 + CO_2$

forsterite jadeite-ureiite solid solution

(5) $10MgSiO_3 + 3MgAl_2O_4 + 3CaMgSi_2O_6$

enstatite spinel diopside

$+ [Na_2CO_3 + Ca(OH)_2]$

carbonatite melt components

$= 2NaCa_2Mg_4Al_3Si_6O_{22}(OH)_2 + 4Mg_2SiO_4 + CO_2$

pargasite forsterite

The net effects of the postulated carbonatite metasomatism are to deplete or eliminate orthopyroxene and spinel, with any residual orthopyroxene being very low in Al_2O_3 content and relict spinel being very Cr rich. There is an accompanying increase in clinopyroxene (including jadeite and ureiite components), in olivine and possibly in pargasite (depending on water activity and bulk composition). Our experimental approach, addition of CO_2 to the assumed products of metasomatism, at pressures slightly above the decarbonation reactions above, produced aluminous orthopyroxene and spinel as predicted.

Pargasitic amphibole is present in the wehrlite starting compositions, but is absent in the super-solidus runs, also as predicted by the above reactions. In sub-solidus experiments at 2.2 GPa, dolomite or magnesite is stable and the co-existing amphibole is edenitic rather than pargasitic, i.e. it is low in Al_2O_3 content (Table 4) and relatively high in SiO_2 and in Na_2O.

Amphibole synthesised by Wallace (1989) at 2.2 GPa and from 950° C (sub-solidus) to 1050° C (in presence of sodic dolomitic melt) in Hawaiian Pyrolite (− 40% olivine composition) is pargasitic with lower SiO_2, higher Al_2O_3 and lower Na_2O than the sub-solidus amphibole in both 71001* and 70965*. The

Table 3 Representative olivine, orthopyroxene and clinopyroxene compositions from the experiments

Run no.	71001* T-3301	T-3197	T-3491	T-3188	70965* T-3315	T-3447	T-3586	T-3327	T-3469
Olivine									
SiO_2	39.49	39.42	41.07	40.27	41.71	40.94	40.95	40.91	41.27
FeO	11.59	11.45	11.32	11.66	10.12	9.64	9.44	10.31	9.72
MnO	0.30	0.33	0.28	0.25	0.26	0.24	0.20	0.25	0.16
MgO	47.52	47.77	48.48	47.70	47.19	48.24	49.33	48.45	48.82
CaO	0.18	0.13	0.20	0.09	0.17	0.41	0.20	0.19	0.26
NiO	–	–	–	–	0.25	0.23	0.35	0.26	0.33
Total	99.08	99.10	101.35	99.97	99.70	99.70	100.47	100.37	100.56
Mg#	87.96	88.14	88.41	87.94	89.26	89.92	90.30	89.33	89.95
Orthopyroxene									
SiO_2	55.10	54.53	55.28	54.90	56.72	54.96	56.47	55.23	56.19
TiO_2	0.13	0.23	0.27	0.23	0.05	0.28	0.05	0.15	0.11
Al_2O_3	1.86	2.92	3.74	3.06	0.98	2.80	1.62	2.90	2.21
FeO	9.57	7.59	7.46	7.31	6.86	6.46	5.98	6.86	6.24
MnO	0.28	0.28	0.24	0.25	0.20	0.15	0.18	0.31	0.20
MgO	30.83	31.92	31.48	30.97	33.49	32.10	33.83	32.38	33.09
CaO	1.05	2.14	1.71	1.89	0.72	1.38	1.11	1.49	1.34
Cr_2O_3	1.25	0.75	1.20	0.98	0.68	0.92	0.68	0.97	0.89
NiO	–	–	–	–	0.18	0.08	0.11	0.12	0.13
Total	100.07	100.36	101.38	99.59	99.88	99.13	100.03	100.41	100.40
Mg#	85.16	88.23	88.26	88.30	89.69	89.85	90.98	89.37	90.43
Clinopyroxene									
SiO_2					53.76	52.46	53.68	53.14	53.78
TiO_2					0.19	0.21	0.15	0.25	0.26
Al_2O_3					1.28	1.74	1.62	2.28	2.33
FeO					3.68	3.87	3.31	3.66	3.24
MnO					0.20	0.18	0.15	0.20	0.11
MgO					17.20	19.03	17.45	17.67	17.40
CaO					20.88	20.16	21.31	19.85	20.46
Na_2O					1.07	0.98	0.82	1.18	1.04
K_2O					0.00	0.04	0.01	0.03	0.01
Cr_2O_3					1.34	1.11	0.87	1.25	1.24
NiO					0.09	0.00	0.04	0.06	0.08
Total					99.69	99.78	99.41	99.57	99.95
Mg#					89.28	89.76	90.38	89.59	90.54

differences are attributed to differences in bulk composition (Na:Ca:Al and CO_2 content).

Amphibole was not detected in any above-solidus experiments, implying sufficient CO_2 to reverse the reaction above involving pargasite and forming sufficient carbonatite melt to either dissolve H_2O or release H_2O into a CO_2-rich fluid phase. Thus in 71001*, at above-solidus conditions, the absence of clinopyroxene and the vesicular nature of the run product (Fig. 2a) are consistent with the presence of excess CO_2 and elimination of both pargasite and diopside. In 70965*, although amphibole was not detected, the charge is not vesicular and the persistence of clinopyroxene suggests that CO_2 was not present in excess.

Apatite was abundant in the 71001* starting composition, and in sub-solidus runs using that composition (T-3172 and T-3301). However, it was absent from all 71001* runs at $T \geqslant 1000^\circ$ C. Apatite was not detected in either the 70965* synthesis run, or in any experimental runs using this composition. Apatite compositions were difficult to determine quantitatively because of the small grain size. However, in addition to CaO and P_2O_5, it contained minor FeO and MgO (≈ 1.2 and 1.5 wt% respectively).

Cr-spinel grains were detected in most runs, but were generally too small (1–2 microns) for accurate microprobe analysis. Semi-quantitative analysis of spinels from run T-3469 indicated a high Cr# of ≈ 61 [where Cr# = atomic 100* Cr/(Cr + Al)].

Carbonate compositions

Carbonate was detected in all runs at $T < 1100^\circ$ C. In runs at 900° C, tiny, interstitial crystals of carbonate were clearly recognizable. In runs at *PT* conditions within the carbonate melt stability field of Wallace and Green (1988) (i.e. $980^\circ\text{C} < T < 1080^\circ\text{C}$ at 2.2 GPa), the carbonate displayed distinctive quench textures (Fig. 2). Carbonate was not found in runs T-3188 and T-3336 (1100 and 1150° C respectively).

Table 4 Representative experimental amphibole compositions

Run no.	T-3301	T-3172	T-3482	T-3315
SiO_2	48.33	48.58	49.73	47.91
TiO_2	0.93	0.74	0.62	0.45
Al_2O_3	7.31	6.50	7.21	7.41
FeO	5.70	5.38	4.05	4.75
MnO	0.11	0.12	0.14	0.12
MgO	21.86	22.72	20.16	21.89
CaO	7.91	9.25	11.80	8.35
Na_2O	4.00	3.49	3.11	3.42
K_2O	0.60	0.44	0.30	0.32
Cr_2O_3	1.39	1.35	1.70	1.29
NiO	–	–	0.06	0.12
P_2O_5	0.24	0.18	0.26	0.20
Total	98.38	98.76	99.14	96.22
Mg#	87.24	88.28	89.87	89.15
Si	6.758	6.773	6.908	6.811
Ti	0.098	0.078	0.065	0.048
Al	1.205	1.068	1.181	1.242
Fe^{3+}	0.467	0.439	0.285	0.395
Fe^{2+}	0.200	0.188	0.186	0.169
Mn	0.013	0.014	0.016	0.014
Mg	4.556	4.721	4.173	4.638
Ca	1.185	1.382	1.756	1.272
Na	1.085	0.943	0.838	0.943
K	0.107	0.078	0.053	0.058
Cr	0.154	0.149	0.187	0.145
Ni	–	–	0.000	0.014
Total	15.828	15.833	15.648	15.749

Sub-solidus carbonate compositions varied between the different starting compositions at identical *PT* conditions. For example, sub-solidus runs using 71001* (T-3301 and T-3172) contained common interstitial Ca-bearing magnesitic carbonate with Mg# = 92.2 (T-3301) and 91.7 (T-3172). However, in the sub-solidus run using the 70965* composition (T-3315), carbonate had a magnesian dolomite composition, with an Mg# of 91.0, and Ca# [where Ca# = 100 Ca/(Ca + Mg + Fe)] of 45.3 (Table 5). The presence of sub-solidus magnesitic carbonate in 71001* runs at 2.2 GPa contrasts with other studies in the peridotite-CO_2-H_2O system (e.g. Wallace and Green 1988), in which dolomite was found. Subsolidus magnesite is however, compatible with the absence of diopsidic clinopyroxene, i.e. diopside is exhausted before magnesite in the reaction magnesite + diopside = enstatite + dolomite. Good mass balance is achieved for the magnesite + amphibole + enstatite + olivine + apatite + spinel, using compositions of analysed phases for both the low CO_2 (1%) and high CO_2 (4.3%) experiments.

In super-solidus runs carbonate melt occurred along grain boundaries, often forming < 10 μm pools at grain-boundary triple junctions. Carbonate melt inclusions were not detected in the San Carlos olivine (discs, or coarsely crushed layers) included in the 71001* runs, although most super-solidus 70965* runs did succeed in trapping some interstitial melt as inclusions in layers of crushed olivine (Fig. 2c). This is possibly because all ($\approx 5\%$) CO_2 was consumed in the 70965* runs, producing $\approx 10\%$ melt. In the 71001* runs, CO_2 was in excess, and insufficient melt was produced to form inclusions. Super-solidus carbonate melt proved extremely difficult to analyse directly by electron microprobe. This was due in part to the nature of its quench aggregates. Backscattered SEM images of unpolished fragments of run material (T-3690 and T-3627) revealed the presence of tiny, tabular, mid-grey dolomitic crystals [Mg# = 79], and spectacular quench growth of a (Na + Mg)-carbonate phase [Mg# = 77; Fig. 1a, b]. Microprobe analyses of these phases are presented in Table 5. The delicate nature of the Na-bearing quench phase raises the strong probability of its mechanical loss during polishing of run products prior to EPMA. In addition, Wallace and

Table 5 Representative experimental carbonate compositions. CM1 is the carbonatite melt composition of Wallace and Green (1988)

Run no.	71001* T-3172	T-3301	T-3197	T-3491	70965* T-3315	T-3447	T-3586	T-3469	Quench phases T-3690 (Na, Mg)-carbonate	T-3690 Dolomite	CM1
SiO_2	0.78	1.77	2.08	5.26	3.82	5.46	8.54	18.16	9.10	0.12	2.94
TiO_2	0.00	0.00	0.12	0.02	0.00	0.02	0.21	0.14	0.28	0.05	0.45
Al_2O_3	0.00	0.00	0.31	0.41	0.00	0.09	1.92	1.12	0.32	0.04	1.95
FeO	6.65	6.27	4.48	2.92	4.13	4.50	4.46	4.67	9.41	5.51	4.61
MnO	0.29	0.49	0.34	0.18	0.25	0.26	0.31	0.26	0.60	0.74	–
MgO	41.29	41.48	22.04	11.35	23.47	17.29	14.38	18.73	17.60	11.49	14.19
CaO	2.92	2.68	29.11	34.33	28.01	29.80	28.11	21.04	9.53	33.03	21.29
Na_2O	0.00	0.00	0.05	0.31	0.04	0.82	0.73	0.63	21.92	0.00	4.99
K_2O	0.00	0.00	0.05	0.10		0.15	0.16	0.10	0.17	0.00	0.35
Cr_2O_3	0.00	0.00	0.75	0.09	0.00	0.02	0.22	0.27	0.09	0.03	0.22
NiO	–	–	–	–	0.00	0.09	0.04	0.12	–	0.00	–
P_2O_5	0.00	0.00	0.43	1.64	0.00	0.42	0.32	0.57	1.96	1.22	0.48
Total	51.93	52.69	59.76	56.61	59.72	58.92	59.40	65.80	70.98	52.43	51.49
Mg#	91.71	92.18	89.76	87.38	91.01	87.26	85.18	87.72	76.92	78.79	84.58

Table 6 Least squares mass balance calculations using phase and bulk compositions for T-3197 (71001*) and T-3586 (70965*). Models 1 and 3 use carbonate melt compositions obtained from direct broad-beam EPMA of quenched melt pools in the run products. Models 2 and 4 use these carbonate melt compositions adjusted to give an insignificant difference between reactants (phases and melt) and product (bulk composition) for Na_2O. CO_2 content of melts estimated from difference between EPMA totals and 100%

	T-3197 Model 1		T-3197 Model 2		T-3586 Model 3		T-3586 Model 4	
Product								
Bulk composition	71001*		71001*		70965*		70965*	
Reactant (modal %)								
Olivine	44.73		44.95		27.25		27.22	
Orthopyroxene	40.08		39.57		47.47		47.51	
Clinopyroxene	0.00		0.00		6.36		6.23	
Spinel	1.58		1.23		1.20		1.01	
Carbonate melt	13.61		14.25		17.71		18.03	
Carbonate melt[a]			10.18[a]				12.88[a]	
	Carbonate melt	Difference = reactant-product	Carbonate melt	Difference = reactant-product	Carbonate melt	Difference = reactant-product	Carbonate melt	Difference = reactant-product
SiO_2	2.08	0.47	1.92	0.27	8.54	0.18	8.23	0.09
TiO_2	0.12	− 0.05	0.11	− 0.05	0.21	− 0.05	0.20	− 0.05
Al_2O_3	0.31	− 0.17	0.29	− 0.20	1.92	− 0.19	1.85	− 0.22
FeO	4.48	− 0.01	4.14	− 0.13	4.46	− 0.24	4.30	− 0.29
MgO	22.04	0.48	20.34	0.30	14.38	0.24	13.87	0.15
CaO	29.11	0.52	26.87	0.38	28.11	0.21	27.09	0.09
Na_2O	0.05	− 1.04	7.75	0.06	0.73	− 0.67	4.34	− 0.01
K_2O	0.05	− 0.11	0.05	− 0.11	0.16	− 0.02	0.15	− 0.02
Cr_2O_3	0.75	0.65	0.69	0.43	0.22	0.33	0.21	0.22
P_2O_5	0.43	− 1.18	0.40	− 1.18	0.32	0.03	0.31	0.03
CO_2	40.24	0.39	37.14	0.20	40.64	0.20	39.46	0.11
$\sum r^2$	3.80		1.99		0.83		0.24	
Distance	1.95		1.41		0.91		0.49	

[a] Melt percentages have been recalculated to allow for 40% olivine removal from the bulk compositions

Green (1988) reported the presence of Na_2CO_3-rich veins in some of their runs, a phase also likely to be extremely fragile and H_2O-soluble, and hence difficult to preserve during polishing. For these reasons run products were carefully impregnated with epoxy before polishing, and water-free polishing oils were used.

Super-solidus carbonate compositions determined by direct, broad-beam EPMA of quenched melt pools are presented in Table 5. These are low SiO_2 (< 18.2 wt %), broadly dolomitic compositions [Ca# $= 42$–66]. They are notable in having very low Na_2O contents (< 1 wt%) compared with 4.99 wt % in the melt of Wallace and Green (1988) (termed CM1 in Table 5). They also have low Al_2O_3, TiO_2, but ubiquitously high Mg#s (85.2–89.8) in close agreement with CM1.

The possibility that the low Na_2O contents in the above carbonate melt compositions are due to loss of a Na-bearing phase during polishing was investigated using mass balance calculations. Table 6 contains the results of least squares calculations on the bulk and phase compositions in runs T-3586 (70965*) and T-3197 (71001*). Calculations were performed using the models ol + opx + sp + carbonate melt = 71001 − 40% ol bulk composition (T-3197), and ol + opx + cpx + sp + carbonate melt = 70965 − 40% ol bulk composition (T-3586). The fits using the directly probed (low Na) carbonate compositions listed in Table 5, are reasonable for most elements (e.g. SiO_2, FeO, MgO and CaO) but poor for Al_2O_3, Cr_2O_3 and P_2O_5 and particularly for Na_2O. In the case of Al_2O_3 and Cr_2O_3 the error may be associated with the unrealistically high Cr_2O_3 content of the 71001* "melt" analysed in T-3197 and to our inability to determine the true equilibrium spinel compositions in these runs due to the fine grain size of spinel. In each case the spinel composition from the relevant nodule (70965 and 71001) was assumed (G.M. Yaxley, unpublished data). The calculations indicated that the ol + opx ± cpx + sp + melt (reactants) sides of the least squares models are significantly deficient in Na_2O, consistent with mechanical loss of this element from quenched melt pools during polishing and possibly also by volatilization under the electron beam during EPMA.

Accordingly, the EPMA-determined carbonate melt compositions were adjusted by adding Na_2O until the fit for this oxide was significantly better (i.e. difference close to 0). Approximately 4.3 wt % Na_2O in the melt in equilibrium with the spinel lherzolite residue in T-3586, and 7.8 wt % Na_2O in the melt in equilibrium with the spinel harzburgite residue in T-3197 resulted in much smaller differences for Na_2O, and improved the overall fit of the models (Table 6).

The foregoing mass balance arguments strongly suggest that considerable Na is lost during polishing

and/or EPMA of experimental charges containing quenched sodic carbonate melts, despite careful precautions to minimize the effect. The calculations provide approximations to the true equilibrium carbonate compositions. These estimations of melt compositions assume only Na_2O-loss, whereas the experiments of Wallace and Green (1988) and T-3690 and T-3627 herein, indicate that lost quench phases may include (Na + Mg)-carbonate, and possibly others as well. Loss of Mg, or other elements (e.g. K, P etc.) has not been accounted for in the calculations. Thus, these results imply sodic (several wt% Na_2O), broadly dolomitic melt compositions (Ca# $\approx$ 0.46–0.54) with Mg#s of $\approx$ 89–90.

Discussion

Simple bulk mixing versus open system metasomatism

The experiments outlined above clearly demonstrate that the compositions of the magnesian wehrlite suite described by Yaxley et al. (1991) are consistent with metasomatic absorption of high Mg# sodic dolomitic melt by refractory lherzolitic or harzburgitic lithosphere at around 2 GPa and 1000° C, and hence support the models of Green and Wallace (1988) and Yaxley et al. (1991). Approximate constraints can be placed on the amount of carbonatite melt absorbed from the mass balance calculations. Adjusting for the olivine removal from our experimental compositions, for 71001* composition, approximately 10% carbonatite melt could have been absorbed by the original harzburgite. In the case of xenolith 70965, the reaction of $\approx$ 13% carbonatite melt (Table 6) with precursor lherzolite could have produced the wehrlite, releasing $\approx$ 6–7 wt % CO_2. It should be noted, however, that simple bulk mixing of refractory harzburgitic or lherzolitic wall-rock with the metal oxide part of a sodic dolomitic carbonatite melt may be an oversimplified view of the metasomatic process. In reality, there may be an open system process, in which wall-rock reactions, of orthopyroxene particularly, and mineral/melt partitioning relationships determine the composition of the metasomatised wall-rock. Compositions may also be modified by a fugitive, volatile-rich melt or fluid, additional to a CO_2-rich vapour phase, which may partially be trapped on grain boundaries (cf. thin films of Si-, Na- and K-rich melts) and may partially escape from the analysed volume.

Implications for CO_2-rich fluid distribution in the lithosphere

The experiments imply that very substantial CO_2-rich fluid fluxes could be generated during carbonatite metasomatism. As discussed above, estimates of $\approx$ 5–7 wt % CO_2 have been lost from the wehrlites 71001* and 70965* if the precursor harzburgite and lherzolite have been correctly reconstructed in Table 6.

Watson and Brenan (1987) have experimentally demonstrated that the wetting angles of CO_2-rich fluids in contact with olivine are substantially greater than 60°, suggesting that permeability of peridotite to such fluids under mantle conditions approaches zero. The ubiquitous presence of CO_2-rich fluid inclusions, marking healed fractures in crystalline phases, is evidence of migration of dense CO_2-rich fluids and consistent with loss of most, but not all, of the high pressure CO_2-rich fluid released by the decarbonation reactions. It is hypothesised that fluid over-pressure at depths of $>$ 60 km is important in fracturing, jointing and local mylonitic planar fractures commonly seen in the lherzolite xenoliths of western Victoria. Fluid-release and wall-rock fracturing will aid magma penetration and the entrainment of wall-rock xenoliths, and magma entering regions of prior-carbonatite metasomatism may become saturated in CO_2-rich fluid. Fluid flux resulting from episodic or continuous carbonatite metasomatic activity may, in these several ways, have significant roles in driving explosive alkali basalt eruptions in an intra-plate volcanic setting.

The role of carbonatites in intra-plate volcanism

Erupted carbonatites occur in continental settings, often associated with volcanism involving highly undersaturated silicate melts (nephelinites, kimberlites, lamproites etc.). They have also been reported from oceanic intra-plate settings such as Cape Verde and the Canary Islands (Allegre et al. 1971; Silva et al. 1981; Barrera et al. 1981; Nelson et al. 1988). In addition, Nelson et al. (1988), Dupuy et al. (1992) and Hauri et al. (1994) have proposed an involvement for carbonatite components in the source regions of many ocean island basalts. The following model suggests how the carbonatitic component could be incorporated into intra-plate volcanics.

Within the pressure range of $\approx$ 2–3 GPa, upwelling partially molten asthenosphere, or ascending asthenospheric diapirs may traverse the stability field of dolomitic carbonatite in equilibrium with amphibole (Wallace and Green 1988), either by cooling or because their initial temperatures are relatively low (path A, Fig. 3). Within this field, initial volatile-rich silicate melts will crystallize mainly amphibole + clinopyroxene, evolving to an intergranular melt of sodic, dolomitic carbonatite. This highly enriched and mobile melt fraction could ascend by porous or dyke flow to around 2 GPa. If it crossed the solidus of the peridotite-CO_2-H_2O system at pressures greater than the decarbonation reaction opx + dol = cpx + ol + CO_2, it would create enriched carbonate-bearing peridotite (path B, Fig. 3). Alternatively it could intersect the solidus at the

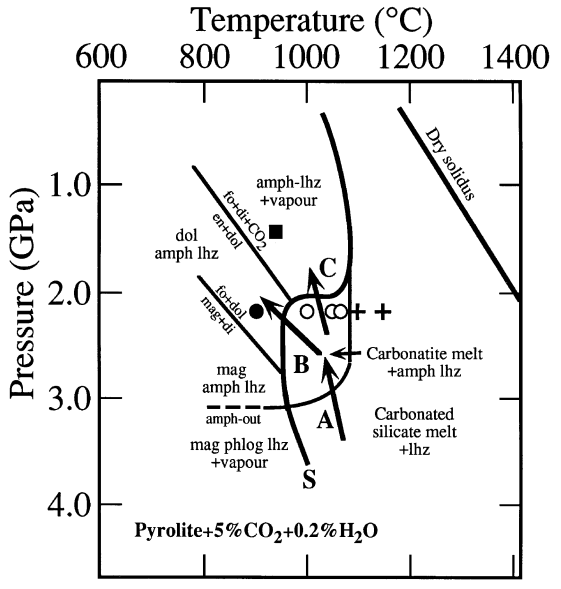

Fig. 3 Phase relations and solidus (*S*) of Hawaiian pyrolite + 5% CO_2 + 0.2% H_2O (H_2O-undersaturated) from Wallace and Green (1988) and Falloon and Green (1989). Dry pyrolite solidus is from Falloon et al. (1988). *PT* window in which sodic dolomitic carbonatite melt is in equilibrium with pargasitic lherzolite, and the field of carbonated undersaturated silicate melt in equilibrium with lherzolitic residue are indicated, as are various sub-solidus stability fields. A carbonated silicate melt could ascend by porous flow or diapiric ascent into the carbonatite melt field (*path A*) and evolve to sodic dolomitic melt by fractionation of amphibole + clinopyroxene. The carbonatite melt could then segregate and rapidly ascend via *path B*, crossing the peridotite solidus, and producing enriched dolomitic peridotite. Alternatively, it could cross the solidus via *path C*, where it would undergo decarbonation reactions with primary peridotite phases, driving harzburgite or lherzolite towards magnesian wehrlite, and releasing substantial fluxes of CO_2-rich fluid. See text for fuller explanation. [*Amph* pargasitic amphibole, *lhz* lherzolite, *dol* dolomite, *mag* magnesite, *phlog* phlogopite, *opx* orthopyroxene, *fo* forsterite, *di* diopside, *en* enstatite. *Black square PT* conditions for carbonate-free syntheses of amphibole wehrlite starting material; *black circle PT* condition which produced sub-solidus magnesite-bearing harzburgite (71001*) or dolomite-bearing lherzolite (70965*) assemblages. *open circles PT* conditions which produced sodic dolomitic carbonatite melt + harzburgite (71001*) or lherzolite (70965*) residues, *crosses PT* conditions which produced silicate melt + harzburgite (71001*) or lherzolite residues (70965*)]

deflection to higher temperatures caused by the decarbonation reaction, and metasomatise the lithosphere in the manner described by Green and Wallace (1988) and Yaxley et al. (1991) (path C, Fig. 3). This would lead to formation of a zone of amphibole + apatite-bearing olivine wehrlite at around 60 km depth. Decarbonation accompanying this process would be substantial and variable, and could cause fracturing and disruption of the lithosphere above this region. Subsequent carbonatite melts would migrate into these fractures, and interact with wall-rock, driving it towards wehrlite, and allowing further ascent of later carbonatite magmas. Decarbonation accompanying metasomatism of the wall-rock would propagate the fracture system towards shallower levels in the lithosphere. Carbonatites ascending through this fracture system, may undergo further decarbonation reactions. For example, the reaction dolomite + 3 diopside = 2 forsterite + 4 calcite + $2CO_2$ (Wyllie and Huang 1976) would increase the calcite component in the melt and modify it towards a calcitic carbonatite (sövite) (Sweeney et al. 1995). Dalton and Wood (1993) have also demonstrated experimentally that reaction of carbonatite melt with an olivine + clinopyroxene assemblage will drive the melt composition to calciocarbonatite at pressures lower than reaction 2. Eruption of the carbonatite to the surface may sometimes occur as a result of continued propagation of the fracture system to shallower levels in the lithosphere. Crustal decarbonation (Sweeney et al. 1995) may generate alkali-rich fenitizing fluids.

Subsequent mafic silicate melts, derived from the asthenosphere may ascend through the metasomatized region via the fracture zones created by interactions between the lithosphere and the carbonatites, and have their compositions modified as well. For example, many intra-plate volcanics have unusually fractionated Zr/Hf values (Dupuy et al. 1992) despite the similarity of melt-residue partition co-efficients for these two elements in basalt-peridotite equilibria. High Zr/Hf appears to be a characteristic otherwise confined to erupted carbonatites (e.g. Nelson et al. 1988) or carbonatite metasomatised peridotite xenoliths (Yaxley et al. 1991; Rudnick et al. 1993). Assimilation of metasomatic clinopyroxene (derived from carbonatite metasomatism) by primitive mafic melts may drive their compositions towards ankaramites (e.g. Barsdell 1988).

Mantle metasomatism by carbonatite melts, over longer times, may convert a significant lithospheric volume (layer) to olivine-rich wehrlite, with the fugitive CO_2 largely lost from the system. If lithospheric melting of this region occurs in a later geodynamic cycle (e.g. re-activation in the mantle wedge overlying a subduction zone) then the wehrlite may act as a source composition for distinctive magmas, i.e. melts in equilibrium with olivine + clinopyroxene ± spinel, and not in equilibrium with orthopyroxene, e.g. ankaramites (G.M. Yaxley, in preparation).

Acknowledgments We gratefully acknowledge technical support provided by Keith Harris, Wis Jablonski and Simon Stevens. Our thanks also go to Drs. Gerhard Brey and Russell Sweeney for constructive reviews.

References

Allegre CJ, Pineau F, Bernat M, Javoy M (1971) Geochemical evidence for the occurrence of carbonatites on Cape Verde and Canary Islands. Nature 233:103

Barrera JL, Fernandez Santin S, Fuster JM, Ibarrola E (1981) Ijolitas-sienitas-carbonatitas de los Fuerteventura (Islas Canarias). Bol Geol Min (Madrid) 92:309–321

Barsdell M (1988) Petrology and petrogenesis of clinopyroxene-rich tholeiitic lavas, Merelave Volcano, Vanuatu. J Petrol 29:927–964

Dalton JA, Wood BJ (1993) The compositions of primary carbonate melts and their evolution through wallrock reaction in the mantle. Earth Planet Sci Lett 119:511–525

Dautria JM, Dupuy C, Takherist D, Dostal J (1992) Carbonate metasomatism in the lithospheric mantle: peridotitic xenoliths from a melilititic district of the Sahara basin. Contrib Mineral Petrol 111:37–52

Dupuy C, Liotard JM, Dostal J (1992) Zr/Hf fractionation in intraplate basaltic rocks: carbonate metasomatism in the mantle source. Geochim Cosmochim Acta 56:2417–2424

Eggler DH, Baker DR (1982) Reduced volatiles in the system C–O–H: implications to mantle melting, fluid formation, and diamond genesis. In: Akimoto S, Manghnani MH (eds) High pressure research in geophysics. Centre for Academic Publications, Tokyo, pp 237–250

Falloon TJ, Green DH (1989) The solidus of carbonated fertile peridotite. Earth Planet Sci Lett 94:364–370

Falloon TJ, Green DH (1990) The solidus of carbonated fertile peridotite under fluid saturated conditions. Geology 18:195–199

Falloon TJ, Green DH, Hatton CJ, Harris KL (1988) Anhydrous partial melting of a fertile and depleted peridotite from 2 to 30 kbar and application to basalt petrogenesis. J Petrol 29:1257–1282

Green DH, Wallace ME (1988) Mantle metasomatism by ephemeral carbonatite melts. Nature 336:459–462

Hauri EK, Shimizu N, Dieu JJ, Hart SR (1994) Evidence for hotspot-related carbonatite metasomatism in the oceanic upper mantle. Nature 365:221–227

Hunter RH, MacKenzie D (1989) The equilibrium geometry of carbonate melts in rocks of mantle composition. Earth Planet Sci Lett 92:347–356

Nelson DR, Chivas AR, Chappell BW, McCulloch MT (1988) Geochemical and isotopic systematics in carbonatites and implications for the evolution of ocean-island sources. Geochim Cosmochim Acta 52:1–17

Rudnick RL, McDonough WF, Orpin A (1992) Northern Tanzanian peridotite xenoliths: a comparison with Kaapvaal peridotites and inferences on metasomatic interactions. In: Meyer HOA, Leonardos O (eds) Kimberlites and related rocks, vol I. Proc 5th Int Kimberlite Conf CPRM Spec Publ 1/A Jan/94, Brasilia, pp 336–353

Rudnick RL, McDonough WF, Chappell BW (1993) Carbonatite metasomatism in the northern Tanzanian mantle: petrographic and geochemical characteristics. Earth Planet Sci Lett 114:463–475

Silva LC, Le Bas MJ, Robertson AHF (1981) An oceanic carbonatite volcano on Santiago, Cape Verde Islands. Nature 294:644–645

Sweeney RJ, Falloon TJ, Green DH (1995) Experimental constraints on the possible mantle origin of natrocarbonatite. In: Bell K, Keller J (eds) Carbonatite Volcanism. Springer-Verlag, Berlin Heidelberg New York, pp. 189–207

Thibault Y, Edgar AD, Lloyd FE (1992) Experimental investigation of melts from a carbonated phlogopite lherzolite: implications for metasomatism in the continental lithospheric mantle. Am Mineral 77:784–794

Wallace ME (1989) Stability of amphibole and carbonate in the upper mantle (unpublished). PhD thesis, Geol Dep Uni Tasmania

Wallace ME, Green DH (1988) An experimental determination of primary carbonatite composition. Nature 335:343–346

Watson EB, Brenan JM (1987) Fluids in the lithosphere, I. Experimentally determined wetting characteristics of CO_2–H_2O fluids and their implications for fluid transport, host rock properties and fluid inclusion formation. Earth Planet Sci Lett 85:497–515

Watson EB, Brennan JM, Baker DR (1990) Distribution of fluids in the continental mantle. In: Menzies MA (ed) Continental lithosphere. Clarendon Press, Oxford, pp 111–125

Wyllie PJ, Huang W-L (1976) Carbonation and melting reactions in the system CaO-MgO-SiO_2-CO_2 at mantle pressures with geophysical and petrological applications. Contrib Mineral Petrol 54:79–107

Yaxley GM, Crawford AJ, Green DH (1991) Evidence for carbonatite metasomatism in spinel peridotite xenoliths from western Victoria, Australia. Earth Planet Sci Lett 107:305–317